

1

2

The early differentiation of Mars inferred from

3

Hf-W chronometry

4

5

6

Thomas S. Kruijer^{1,2}, Thorsten Kleine¹, Lars E. Borg², Gregory A. Brennecka¹, Anthony J.
Irving³, Addi Bischoff¹, Carl B. Agee⁴

8

9

10

¹Institut für Planetologie, University of Münster, Wilhelm-Klemm-Strasse 10, 48149, Münster,
Germany.

11

12

13

²Nuclear and Chemical Sciences Division, Lawrence Livermore National Laboratory, Livermore,
California 94550, USA.

14

15

16

³Department of Earth and Space Sciences, University of Washington, Seattle, Washington 98195,
USA.

17

18

19

⁴Institute of Meteoritics, University of New Mexico, Albuquerque, New Mexico 87131, USA.

20

21

22

23

Revised manuscript prepared for *Earth and Planetary Science Letters*

24

Version: 23 June 2017

25

26

Abstract: 215 words

27

Main text: 5941 words, 45 citations, 7 figures, 1 table

28

Supplementary Material: 2520 words, 3 figures, 5 tables

29

30 **Abstract**

31 Mars probably accreted within the first 10 million years of Solar System formation and likely
32 underwent magma ocean crystallisation and crust formation soon thereafter. To assess the nature and
33 timescales of these large-scale mantle differentiation processes we applied the short-lived ^{182}Hf – ^{182}W
34 and ^{146}Sm – ^{142}Nd chronometers to a comprehensive suite of martian meteorites, including several
35 shergottites, augite basalt NWA 8159, orthopyroxenite ALH 84001 and polymict breccia NWA 7034.
36 Compared to previous studies the ^{182}W data are significantly more precise and have been obtained for
37 a more diverse suite of martian meteorites, ranging from samples from highly depleted to highly
38 enriched mantle and crustal sources. Our results show that martian meteorites exhibit widespread
39 $^{182}\text{W}/^{184}\text{W}$ variations that are broadly correlated with $^{142}\text{Nd}/^{144}\text{Nd}$, implying that silicate differentiation
40 (and not core formation) is the main cause of the observed $^{182}\text{W}/^{184}\text{W}$ differences. The combined ^{182}W –
41 ^{142}Nd systematics are best explained by magma ocean crystallisation on Mars within ~20–25 million
42 years after Solar System formation, followed by crust formation ~15 million years later. These ages
43 are indistinguishable from the I-Pu-Xe age for the formation of Mars' atmosphere, indicating that the
44 major differentiation of Mars into mantle, crust, and atmosphere occurred between 20 and 40 million
45 years after Solar System formation and, hence, earlier than previously inferred based on Sm-Nd
46 chronometry alone.

47

48 **Key words:** martian meteorites, Hf-W chronometry, Sm-Nd chronometry, planetary differentiation,
49 magma ocean, crust formation

50

51 **1 Introduction**

52 The early evolution of Mars probably involved large-scale melting and core formation, followed
53 by magma ocean crystallisation and crust formation (e.g. Elkins-Tanton, 2005; Mezger et al., 2013).
54 The timescales of these processes can be quantified through the application of the short-lived ^{182}Hf –
55 ^{182}W [half-life = 8.9 million years (Ma)] and ^{146}Sm – ^{142}Nd (half-life = 103 Ma) systems to martian

56 meteorites, which derive from compositionally distinct sources that were established during the early
57 differentiation of Mars. The mantle sources of martian meteorites are thought to comprise mafic
58 cumulates and late-stage crystallisation products of a magma ocean (Borg et al., 1997; Borg and
59 Draper, 2003; Elkins-Tanton, 2008, 2005), as well as crust (Agee et al., 2013; Humayun et al., 2013).
60 These distinct reservoirs have different Hf/W and Sm/Nd ratios, ultimately leading to variations in
61 radiogenic ^{182}W and ^{142}Nd within the martian mantle and crust. Thus, the ^{182}W and ^{142}Nd compositions
62 of martian meteorites from distinct sources reflect Hf/W and Sm/Nd fractionations during the earliest
63 evolution of Mars and as such can be used to constrain the timescales of magma ocean processes and
64 crust formation.

65 Several studies have shown that large radiogenic ^{182}W and ^{142}Nd variations exist within Mars
66 (Borg et al., 2016, 1997; Brennecka et al., 2014; Caro et al., 2008; Debaille et al., 2007; Foley et al.,
67 2005; Kleine et al., 2004; Lee and Halliday, 1997). For instance, nakhlites display some of the most
68 radiogenic ^{142}Nd and ^{182}W compositions yet reported among martian meteorites, indicating source
69 formation within ~25 Ma of Solar System formation (Harper et al., 1995; Kleine et al., 2004; Foley et
70 al., 2005; Debaille et al., 2009). Similarly, early studies on shergottites suggested that Mars primordial
71 differentiation occurred at about 20–60 Ma after Solar System formation (Borg et al., 2003; Kleine et
72 al., 2004; Foley et al., 2005). However, mainly driven by improvements in the analytical precision of
73 $^{142}\text{Nd}/^{144}\text{Nd}$ measurements, subsequent studies demonstrated that shergottites define a precise ^{142}Nd -
74 ^{143}Nd model age of 63 ± 6 Ma after Solar System formation (Borg et al., 2016). The significance of this
75 age, and whether the ^{142}Nd - ^{143}Nd systematics of shergottites record a single differentiation event is
76 debated, however. As such, the ^{142}Nd - ^{143}Nd data for shergottites have also been interpreted to record a
77 prolonged interval of magma ocean crystallisation on Mars, lasting between ~30–100 Ma after Solar
78 System formation (Debaille et al., 2007).

79 One potential issue in the chronological interpretation of ^{142}Nd - ^{143}Nd systematics is the presence
80 of nucleosynthetic Nd isotope variations that arise through the heterogeneous distribution of presolar
81 matter at the bulk meteorite and planetary scale (Burkhardt et al., 2016). For instance, recent studies
82 have shown that the ~10–20 parts-per-million ^{142}Nd difference observed between chondrites and
83 terrestrial samples (Boyet and Carlson, 2005) reflects nucleosynthetic Nd isotope heterogeneity

84 between chondrites and the Earth (Burkhardt et al., 2016; Bouvier and Boyet, 2016), rather than an
85 early Sm/Nd fractionation and subsequent radiogenic ingrowth from short-lived ^{146}Sm . The ^{142}Nd
86 difference between terrestrial samples and chondrites, therefore, does not provide a record of an early
87 differentiation of the silicate Earth. This example highlights that quantifying the extent of
88 nucleosynthetic Nd isotope variations is essential for using the ^{146}Sm - ^{142}Nd system to obtain
89 meaningful ages for early differentiation processes. For Mars the extent of nucleosynthetic Nd isotope
90 anomalies is not well known, however, and this may impact the chronology of Mars' early
91 differentiation inferred from ^{146}Sm - ^{142}Nd systematics. For instance, assuming an ordinary chondrite-
92 like bulk $^{142}\text{Nd}/^{144}\text{Nd}$ for Mars provides a ~30 Ma model age for the formation of the source of
93 depleted shergottites (Debaille et al., 2007), whereas this age changes to ~60 Ma if an Earth-like
94 $^{142}\text{Nd}/^{144}\text{Nd}$ is assumed for bulk Mars (Borg et al., 2016). Thus, the aforementioned uncertainties in the
95 ^{146}Sm - ^{142}Nd timescale for Mars' early differentiation at least partially reflect uncertainties in the ^{142}Nd
96 composition of bulk Mars.

97 The Hf-W chronometer is ideally suited to investigate the duration of magma ocean
98 differentiation on Mars and to distinguish between an early differentiation at ~30 Ma and a later
99 differentiation at ~60 Ma after Solar System formation. This is because owing to the much shorter
100 half-life of ^{182}Hf compared to ^{146}Sm , significant ^{182}W variations can only be produced within the first
101 ~50 Ma of the Solar System (e.g., Kleine et al., 2009). Thus, if the martian magma ocean crystallized
102 at ~60 Ma as suggested by a ^{142}Nd - ^{143}Nd isochron for shergottites (Borg et al., 2016), then these
103 meteorites should all have the same ^{182}W composition. Conversely, if Mars' early differentiation
104 largely occurred at ~30 Ma, then there should be ^{182}W variations among the shergottites. Published
105 ^{182}W data for shergottites do not show resolvable ^{182}W variations (Foley et al., 2005; Kleine et al.,
106 2004; Lee and Halliday, 1997) and, therefore, seem to be consistent with differentiation of Mars at
107 ~60 Ma after Solar System formation. However, the precision of the ^{182}W measurements achievable at
108 the time of these earlier studies was significantly lower than at present and was insufficient for
109 resolving potential ^{182}W variations among the shergottites formed from relatively young source
110 regions.

111 To assess the extent of ^{182}W variations in the martian mantle, and to better constrain the
112 timescales of Mars' early differentiation, we obtained high-precision ^{182}W data for a comprehensive
113 suite of martian meteorites, including samples derived from some of the most enriched and depleted
114 sources known on Mars. To help interpret the ^{182}W data in terms of differentiation timescales, we also
115 obtained high-precision ^{142}Nd data for some of the same samples, coupled with data for non-
116 radiogenic Nd isotopes to assess whether Mars shows a nucleosynthetic Nd isotope anomaly relative
117 to Earth. Combined, these data provide new insights into the timescales of core formation, magma
118 ocean crystallisation, and crust formation on Mars.

119

120 **2 Samples and analytical methods**

121 Samples selected for this study include several shergottites (5 enriched, 3 intermediate, 5
122 depleted), augite basalt Northwest Africa (NWA) 8159, orthopyroxenite Allan Hills (ALH) 84001,
123 and polymict breccia NWA 7034. The last two samples derive from the most incompatible trace
124 element-enriched sources, whereas Tissint and NWA 7635 derive from the most depleted sources
125 known on Mars (Agee et al., 2013; Brennecka et al., 2014; Humayun et al., 2013; Lapen et al., 2017,
126 2010; Nyquist et al., 2016). Note that NWA 7034 is a breccia containing matrix and clasts of
127 numerous different lithologies (Agee et al., 2013; Humayun et al., 2013). The bulk sample analysed
128 here is relatively typical for NWA 7034, and represents a mixture of various clasts and matrix. All
129 samples were received as rock fragments. Their surfaces were abraded to remove any potential
130 terrestrial contamination, and the samples (~0.2-2.5 g) were then ultrasonically cleaned and rinsed
131 with ethanol, and subsequently crushed and ground to a fine powder in an agate mortar.

132 The analytical techniques for sample digestion, chemical separation of W, and W isotope ratio
133 measurements by MC-ICPMS are based on previously developed procedures (Kruijer et al., 2015,
134 2014) and are described in detail in the online Supplementary Material. In brief, the martian meteorite
135 samples and terrestrial rock standards (~0.2-0.5 g) were digested in HF-HNO₃ (2:1) at 130-150 °C on
136 a hotplate for 2-3 days. When samples quantities of >0.5g were needed to obtain sufficient W, powder
137 splits of <0.5 g were digested in separate vials. Tungsten was separated from the sample matrix using

138 a two-stage anion exchange chromatography in HCl-HF media (Kleine et al., 2012; Kruijjer et al.,
139 2015, 2014). Total procedural yields were ~75-100%, and total blanks correspond to ~50-100 pg W
140 and were negligible given the amounts of W analysed (~30-150 ng).

141 The W isotope compositions were measured to high precision using a ThermoScientific® Neptune
142 Plus MC-ICPMS in the Institut für Planetologie at the University of Münster (Kruijjer et al., 2015,
143 2012). Instrumental mass bias was corrected by internal normalization to $^{186}\text{W}/^{184}\text{W} = 0.92767$ using
144 the exponential law. Note that we only used $^{186}\text{W}/^{184}\text{W}$ -normalised data and avoided normalisations
145 involving ^{183}W ; the latter can be biased by a small analytical effect on ^{183}W introduced during sample
146 preparation (see Section 3 and Supplementary Material), as observed in this and multiple earlier
147 studies (e.g., Cook and Schönbacher, 2016; Kruijjer et al., 2012; Willbold et al., 2011). A single W
148 isotope measurement comprised 200 cycles of 4.2 s integration time each. The W isotope analyses of
149 samples are reported as ϵ -unit (*i.e.*, 0.01%) deviations from the mean values of the bracketing
150 standards (Alfa Aesar® metal, batch no. 22312) obtained in one analytical session. The accuracy and
151 reproducibility of the W isotope measurements were assessed by repeated analyses of terrestrial rock
152 standards (BHVO-2, BCR-2), which were digested and processed through the full chemical separation
153 and analysed alongside the martian samples. The mean ^{182}W obtained for multiple analyses of the
154 terrestrial rock standards yields $^{182}\text{W} = 0.01 \pm 0.10$ (2s.d., $N=42$, Fig. 1), demonstrating the high level
155 of precision achieved for a single W isotope analysis consuming as little as ~30 ng W. Note that the
156 *external* reproducibility of $\pm 0.10 \epsilon^{182}\text{W}$ (2 s.d.) obtained here is significantly better than that reported
157 in earlier W isotope studies of martian meteorites (Foley et al., 2005; Kleine et al., 2004), where the
158 external precision was typically on the order of $\pm 0.5 \epsilon^{182}\text{W}$ (2 s.d.).

159 For the analyses of Nd isotope compositions in some of the same samples, we recombined the
160 saved matrix aliquots from the W separation procedure described above. Neodymium was then
161 separated through several ion exchange chromatography steps as described in Borg et al. (2016), and
162 analysed using the Triton TIMS at Lawrence Livermore National Laboratory following previously
163 established procedures (Borg et al., 2016; Burkhardt et al., 2016; more details given in the
164 Supplementary Material, Section S5). Neodymium isotope compositions were corrected for
165 instrumental mass fractionation by internally normalizing to $^{146}\text{Nd}/^{144}\text{Nd} = 0.7219$ using the

166 exponential law, and are reported in ^{142}Nd as the parts-per 10^4 deviations from terrestrial standard
167 values. Total procedural yields for Nd obtained using this procedure were 60-95% and total blanks
168 were approximately 50 pg Nd, which is inconsequential given the amounts of Nd analysed (~500 ng
169 Nd).

170

171 **3 Results**

172 The investigated samples shows large and well-resolved ^{182}W variations from approximately
173 +0.1 (ALH 84001) to approximately +1.8 (NWA 7635) (Fig. 2a, Table 1), indicating that the total
174 spread in ^{182}W is much larger than found for shergottites by previous studies (Fig. 2b; Foley et al.,
175 2005; Kleine et al., 2004; Lee and Halliday, 1997). In particular, in contrast to earlier work, we find
176 that different groups of shergottites exhibit distinct ^{182}W values. The enriched shergottites have a
177 uniform ^{182}W of 0.37 ± 0.05 (95% conf., $n=5$), whereas the depleted shergottites exhibit more elevated
178 and more variable ^{182}W from *ca.* +0.8 to +1.8. The larger range of ^{182}W values not only reflects the
179 higher precision of our measurements compared to previous investigations, but also the more diverse
180 sample suite examined here that included several meteorites for which ^{182}W data had not previously
181 been reported, such as NWA 7635, Tissint, NWA 8159 and NWA 7034 (Fig. 2). Both the terrestrial
182 rock standards and some martian samples exhibit small deficits in measured ^{183}W (Tables S1, S2).
183 These offsets have been observed in several previous studies and are attributed to a small mass-
184 independent fractionation affecting only ^{183}W that is induced during sample preparation (e.g., Budde et
185 al., 2015; Cook and Schönbachler, 2016; Kruijer et al., 2012; Willbold et al., 2011), most likely by a
186 nuclear field shift effect induced during incomplete dissolution of W in Savillex beakers (Cook and
187 Schönbachler, 2016). Nevertheless, this ^{183}W -effect does not modify ^{182}W values normalized to
188 $^{186}\text{W}/^{184}\text{W}$, which is the normalization used throughout this study.

189 The ^{142}Nd compositions of some of the same martian samples shows a similar spread as observed
190 in previous work (Borg et al., 2016, 1997; Caro et al., 2008; Debaille et al., 2007; Foley et al., 2005)
191 (Tables 1, S3). However, ^{142}Nd values obtained for ALH 84001 and NWA 7034 (*ca.* -0.30 and *ca.* -
192 0.45), are the lowest values determined so far for martian meteorites; these unradiogenic ^{142}Nd

193 compositions are consistent with derivation of these samples from the most enriched sources known
194 on Mars. The non-radiogenic Nd isotope data (*i.e.*, isotope ratios not affected by radioactive decay)
195 collected in this study and also in Borg et al. (2016) show considerable scatter (Fig. S1), making it
196 difficult to reliably assess as to whether the Nd isotopic composition of Mars is different from that of
197 the Earth. Nevertheless, when mean values and their associated 95% conf. limits are calculated
198 (N=16, Table S3), hints of small excesses become apparent for ^{148}Nd ($+0.05\pm 0.02$) and ^{150}Nd
199 ($+0.14\pm 0.10$), but not for ^{145}Nd ($+0.02\pm 0.03$). The larger scatter of these data compared to previous
200 work (Burkhardt et al., 2016) reflects the shorter duration and lower intensity of the Nd measurements
201 of the present study, caused by the smaller mass of sample available. While this is inconsequential for
202 resolving the large ^{142}Nd variations among martian meteorites, it makes detecting small
203 nucleosynthetic Nd isotope anomalies more difficult.

204

205 **4 Discussion**

206 **4.1 Origin of ^{182}W variations and Hf-W age of core formation**

207 Utilizing the Hf-W system to date core formation on Mars requires knowledge of the ^{182}W
208 composition of the bulk martian mantle, that is, the martian mantle composition set solely by core
209 formation. Previous studies have estimated this value using the co-variation of ^{182}W and ^{142}Nd
210 (Kleine et al., 2004; Foley et al., 2005; Mezger et al., 2013). Because silicate differentiation leads to
211 correlated ^{182}W - ^{142}Nd variations, the ^{182}W of samples having the ^{142}Nd of bulk Mars should represent
212 the ^{182}W of the bulk martian mantle (Kleine et al., 2004; Foley et al., 2005). Despite demonstrating
213 significant variations in ^{142}Nd isotopic compositions, previous data for shergottites did not show large
214 ^{182}W variations (Foley et al., 2005; Kleine et al., 2004), yielding precise estimates of the ^{182}W of the
215 bulk martian mantle, with values between 0.34 ± 0.07 and 0.45 ± 0.15 (Foley et al., 2005; Kleine et al.,
216 2004). By contrast, the results obtained in the present study reveal significant ^{182}W variations among
217 shergottites (Fig. 1) that show a general positive trend with ^{142}Nd (Fig. 3). In particular, meteorites
218 with the most enriched source characteristics (as given e.g. by La/Sm) and lowest ^{182}W also show low
219 ^{142}Nd (NWA 7034, ALH 84001), whereas those derived from depleted sources with higher ^{182}W

220 show higher ^{142}Nd (NWA 7635, Tissint). Whereas variations in ^{182}W can be caused by both core
221 formation and silicate differentiation, ^{142}Nd variations can only be produced by silicate differentiation.
222 The positive trend between ^{182}W and ^{142}Nd , therefore, implies that these isotope variations are caused
223 by the same process, so that the ^{182}W differences predominantly reflect silicate differentiation and not
224 core formation. Nonetheless, in spite of this general ^{182}W vs. ^{142}Nd trend, there is considerable scatter
225 about the trend, indicating that the ^{182}W vs. ^{142}Nd systematics cannot be caused by a single episode of
226 differentiation within the martian mantle – this will be discussed in detail further below (Section 4.2).

227 As in previous studies, the ^{182}W of the bulk martian mantle can be determined from the ^{182}W -
228 ^{142}Nd variation combined with an estimate of the bulk martian mantle ^{142}Nd (e.g. Mezger et al.,
229 2013). The latter is uncertain, however, due to nucleosynthetic Nd isotope heterogeneity among the
230 terrestrial planets and chondrites (Burkhardt et al., 2016). Currently proposed ^{142}Nd values for bulk
231 Mars range from $^{142}\text{Nd} = -0.06$ (Borg et al., 2016) down to the composition measured for ordinary
232 chondrites (*i.e.*, $^{142}\text{Nd} = -0.18$) (Debaille et al., 2007). However, over this range of values there is
233 essentially no variability in ^{182}W among the martian meteorites (*i.e.*, the enriched shergottites and
234 NWA 7042) (Fig. 3). Thus, we take the mean $^{182}\text{W} = +0.37 \pm 0.04$ (95% conf.) of these shergottites to
235 represent the ^{182}W of the bulk martian mantle. This value is consistent with but more precise than the
236 previous estimates summarized above (Foley et al., 2005; Kleine et al., 2004).

237 As the bulk martian mantle ^{182}W deduced in the present study is not different from those inferred
238 previously, the calculated Hf-W model ages for core formation do not change. Nevertheless, core
239 formation ages are briefly reviewed below to provide an estimate for the duration of Mars' accretion
240 and core formation. Assuming that bulk silicate Mars has a ^{182}W value of $+0.37 \pm 0.04$ and a $^{180}\text{Hf}/^{184}\text{W}$
241 ratio of 4.0 ± 0.5 (Dauphas and Pourmand, 2011) yields a two-stage model age for core formation of
242 4.1 ± 2.7 Ma. The two-stage Hf-W model age assumes that core formation occurred in a single
243 instant, but this assumption may not be valid for larger bodies like Mars, in which metal segregation
244 likely occurred by several distinct events as accretion proceeded. In this case, a more realistic age is
245 obtained by assuming continuous core formation and an exponentially decreasing accretion rate
246 (Harper and Jacobsen, 1996). In this model, a mean life of accretion, corresponding to 63% growth, of
247 $\tau = 2.4^{+1.3}_{-1.5}$ Ma is obtained, consistent with a previous estimate of $1.8^{+0.9}_{-1.0}$ Ma for 44% growth from

248 Dauphas and Pourmand (2011). In this model, ~90% of Mars' growth would have been completed by
249 ~6 Ma after Solar System formation. These age calculations assume complete metal-silicate
250 equilibration during core formation, but as to whether this has always been the case is not known. For
251 instance, if Mars formed as a stranded planetary embryo, then most of its mass was added by small
252 planetesimals, in which case complete metal-silicate equilibration seems likely. If, however, Mars'
253 accretion involved giant impacts, then it is possible that the metal cores of these impactors did not
254 fully equilibrate within the martian mantle before entering the core (e.g., Morishima et al., 2013). In
255 this case the true core formation time would be younger than the ages calculated above (Mezger et al.,
256 2013; Nimmo and Kleine, 2007). For instance, assuming the degree of metal-silicate equilibration was
257 only 50%, then t_{core} would change to ~5 Ma, meaning that ~90% of Mars' mass would have accreted by
258 ~10 Ma after Solar System formation (Mezger et al., 2013). Taken together, the Hf-W systematics
259 indicate that most of Mars' accretion history was probably completed within the first ~10 Ma of Solar
260 System history. This age provides a quite robust estimate for the accretion rate of Mars, unless the
261 Hf/W ratio of the martian mantle is significantly higher than currently estimated. Although currently
262 available data seem to preclude this possibility, the data upon which this estimate is based were
263 obtained on only a small number of samples and using different analytical techniques. As such it
264 would be useful for future studies to determine the Hf/W ratio of the martian mantle on a larger set of
265 samples and using a common high-precision analytical method.

266

267 **4.2 Using combined ^{182}W - ^{142}Nd systematics to date silicate differentiation**

268 In order to utilize the ^{182}W and ^{142}Nd data for determining differentiation timescales, we assessed
269 the extent of Hf/W and Sm/Nd fractionations within the martian mantle using magma ocean
270 crystallisation models (Borg and Draper, 2003; Debaille et al., 2008; Elkins-Tanton, 2005). In this
271 modelling the generation of *depleted* martian mantle sources was simulated through the sequential
272 crystallisation of several cumulate packages from the magma ocean (Lodders and Fegley, 1997; Borg
273 and Draper, 2003; Supplementary Material). In this model, the residual liquid left behind after magma
274 ocean crystallisation then represents the *enriched* mantle end member composition. The bulk martian
275 mantle, *i.e.*, the starting composition of the model, was assumed to have a chondritic $^{147}\text{Sm}/^{144}\text{Nd}$ of

276 0.1960 (Jacobsen and Wasserburg, 1980; Bouvier et al., 2008) and a $^{180}\text{Hf}/^{184}\text{W}$ of 4.0 ± 0.5 (Dauphas
277 and Pourmand, 2011). For the modelling we used published crystal-melt partition coefficients for Sm,
278 Nd, Hf, and W (Borg and Draper, 2003; Righter and Shearer, 2003; Snyder et al., 1992) (Table S4),
279 and the high-pressure (~15 GPa) cumulate crystallisation assemblage from Borg and Draper (2003),
280 corresponding to a magma ocean depth of ~1350 km (Borg and Draper, 2003; Righter and Chabot,
281 2011; Righter and Shearer, 2003). The modelling shows that the cumulate packages have $^{147}\text{Sm}/^{144}\text{Nd}$
282 ratios from 0.282 to 0.528 and $^{180}\text{Hf}/^{184}\text{W}$ ratios from 12 to 23, corresponding to 5 to 98% crystallised
283 solids (Table S5). The weighted mean values for the cumulate packages used here correspond to
284 $^{147}\text{Sm}/^{144}\text{Nd} \cdot 0.291$ and $^{180}\text{Hf}/^{184}\text{W} \cdot 14$, in good agreement with previous estimates (Borg and Draper,
285 2003; Debaille et al., 2008; Foley et al., 2005; Righter and Shearer, 2003). For the range in enriched
286 end-member compositions, we used the $^{147}\text{Sm}/^{144}\text{Nd}$ of 0.157-0.170 and $^{180}\text{Hf}/^{184}\text{W}$ of 1.19-1.83
287 modelled for 98 to 99.5% trapped liquid. Using the $^{180}\text{Hf}/^{184}\text{W}$ and $^{147}\text{Sm}/^{144}\text{Nd}$ ratios obtained, the ^{182}W
288 and ^{142}Nd evolution were calculated for enriched and depleted mantle sources formed at different
289 times after Solar System formation.

290 The results of the modelling demonstrate that the ^{182}W variations as well as the coupled ^{142}Nd -
291 $\epsilon^{182}\text{W}$ variations of martian meteorites are reproduced for differentiation ages between ~20 and ~40
292 Ma after Solar System formation (Fig. 3, 4), where the isotopic compositions of ALH 84001, Tissint,
293 and NWA 7635 require differentiation as early as ~20–25 Ma after Solar System formation. Note that
294 especially the large ^{182}W variations observed among the martian meteorites require such an early
295 differentiation of Mars. For instance, producing the $\epsilon^{182}\text{W}$ excess of ~+1.8 for NWA 7635 at 60 Ma
296 after Solar System formation (*i.e.*, the age for martian differentiation previously inferred from ^{146}Sm -
297 ^{142}Nd systematics of shergottites) would require a $^{180}\text{Hf}/^{184}\text{W}$ ratio of ~135 for the source of this sample
298 (Fig. 4). By contrast, our modelling, as well as previous work (Foley et al., 2005; Kleine et al., 2004;
299 Righter and Shearer, 2003), shows that mafic cumulates of a martian magma ocean have $^{180}\text{Hf}/^{184}\text{W}$
300 ratios that are much lower and typically are between ~12 and ~23; only garnet/majorite has a higher
301 $^{180}\text{Hf}/^{184}\text{W}$ ratio of ~128 (Table S5). However, a mantle source consisting exclusively of garnet is not
302 appropriate for the shergottites, whose source consists of a mixture of olivine, orthopyroxene,
303 clinopyroxene, garnet and ilmenite (Borg and Draper, 2003; Debaille et al., 2008), yielding a bulk

304 $^{180}\text{Hf}/^{184}\text{W}$ ratio of only ~14. Thus, for the modelled range of $^{180}\text{Hf}/^{184}\text{W}$ ratios in the shergottite sources,
305 the large ^{182}W variations observed among the shergottites require source formation much earlier than
306 previously inferred solely based on ^{142}Nd systematics. Of note, using different bulk martian mantle
307 ^{182}W compositions (from +0.25 to +0.5), crystallisation sequences and/or cumulate packages yields
308 very similar silicate differentiation ages for Mars (see Supplementary material, Fig. S2). Furthermore,
309 using individual cumulate packages as the depleted end member composition in the magma ocean
310 model (Fig. S3, Table S5) yields differentiation ages that are consistent with those derived when the
311 weighted mean cumulate compositions is used (Fig. 3). Thus, the differentiation ages for the martian
312 mantle inferred here do not depend on a particular magma ocean model or bulk composition.

313 Further evidence for an early differentiation of Mars comes from the incompatible trace element
314 –enriched nature of the sources of ALH 84001 and NWA 7034. These meteorites exhibit lower ^{182}W
315 and ^{142}Nd than the bulk martian mantle and so must derive from sources with Hf/W and Sm/Nd ratios
316 below those of the bulk mantle (Fig. 3, 4). Note that although NWA 7034 is a breccia that contains a
317 meteoritic component added during impacts on the martian surface (Humayun et al., 2013), the effect
318 of this meteorite contamination is very small, <0.03 ^{182}W (see Supplementary Material). Thus, the
319 low ^{182}W of NWA 7034 cannot reflect meteorite contamination, but instead indicates derivation from
320 a source (or sources) characterized by low-Hf/W ratios. Since the $^{180}\text{Hf}/^{184}\text{W}$ of the bulk martian
321 mantle is only 4.0 ± 0.5 (Dauphas and Pourmand, 2011), there is only a very limited range of possible
322 Hf/W ratios for the sources of ALH 84001 and NWA 7034, and so the inferred source formation ages
323 are essentially independent on the partition coefficients and bulk mineralogy used for modelling
324 magma ocean crystallisation. This makes the formation ages for the ALH 84001 and NWA 7034
325 sources of ~25-40 Ma quite robust (Fig. 3, 4). Note that because NWA 7034 is a breccia, its isotopic
326 composition may not reflect derivation from a single source (Nyquist et al., 2016). Consequently, the
327 bulk sample of NWA 7034 measured here could potentially represent a mixture of components with
328 lower and higher ^{182}W and ^{142}Nd than that measured for the bulk sample. If this is the case, then the
329 component with lower ^{182}W and ^{142}Nd would require an even earlier source formation time than the
330 bulk sample. Thus, W isotope analyses of individual clasts from NWA 7034 may allow even more
331 precise determination of the timing of crust formation on Mars.

332 An important observation from the new isotopic data is that the martian meteorites analysed here
333 do not define a single mixing array in ^{142}Nd vs. ^{182}W space (Fig. 3). Such ^{182}W - ^{142}Nd systematics can
334 potentially be explained by variable mixing between intermediate magma ocean differentiation
335 products (*i.e.*, individual cumulate packages) formed contemporaneously (Table S5; Fig. S3).
336 However, mixing lines for some individual cumulate packages fail to reproduce the alignment of the
337 data in ^{142}Nd - ^{182}W space, and also cannot explain the ^{142}Nd - ^{182}W composition of ALH 84001 (Fig. S3,
338 see Supplementary Material). Instead, rather than by instantaneous differentiation, the ^{182}W - ^{142}Nd
339 systematics are most easily explained by a more prolonged interval of differentiation between ~20 and
340 ~40 Ma after Solar System formation (Fig. 3). For instance, the combined ^{182}W - ^{142}Nd systematics of
341 ALH 84001 appear to require source formation at ~20-25 Ma after CAI formation, whereas the source
342 of NWA 7034 appears to have formed later at ~40 Ma after CAIs. It is noteworthy that combined
343 ^{147}Sm - ^{143}Nd and ^{176}Lu - ^{176}Hf systematics have been used to argue that the source of ALH 84001 contains
344 trapped residual liquid of a magma ocean (Lapen et al., 2010), whereas the source of NWA 7034 is
345 thought to be martian crust rather than residual liquid of a magma ocean (Agee et al., 2013; Humayun
346 et al., 2013; Nyquist et al., 2016). Thus, one possibility to account for the disparate ^{182}W - ^{142}Nd
347 systematics of ALH 84001 and NWA 7034 is that the formation age of the ALH 84001 source
348 inferred here records the timing of the final stage of magma ocean crystallisation at ~20–25 Ma after
349 Solar System formation, whereas the later formation age of the NWA 7034 source at ~40 Ma inferred
350 here reflects crust formation by means of re-melting of the mantle, perhaps triggered by cumulate
351 overturn (Debaille et al., 2009; Elkins-Tanton, 2005). Similarly, re-melting and cumulate overturn in
352 the mantle also provides an explanation for the slightly younger source formation ages of some
353 depleted shergottites (DaG 476, SaU 005) and augite basalt NWA 8159 in comparison to the most
354 depleted shergottites Tissint and NWA 7635 (Fig. 3, 4). A corollary of the above is that the initial
355 solidification of the martian mantle must have preceded these re-melting and crust formation events,
356 and so regardless of whether the enriched sources reflect trapped liquid of a magma ocean or martian
357 crust, our results indicate that magma ocean crystallisation on Mars occurred ~20–25 Ma after Solar
358 System formation.

359 This age for magma ocean crystallisation is similar to the ~23 Ma source formation age of
360 nakhlites as inferred from their ^{182}W - ^{142}Nd composition (Debaille et al., 2009; Foley et al., 2005). The
361 nakhlites are thought to derive from deep mantle sources comprised of cumulates formed during the
362 onset of magma ocean solidification (Debaille et al., 2009). Thus, these data considered together
363 suggest that deep and shallow regions of the magma ocean crystallized about contemporaneously at
364 ~20–25 Ma, followed by crust formation until at least ~40 Ma after Solar System formation (Fig. 5).
365 Finally, the differentiation timescales for Mars inferred here are also consistent with ^{129}I - ^{244}Pu -Xe
366 systematics of martian meteorites that indicate an early I/Pu fractionation related to intensive, large-
367 scale magmatic activity in the martian mantle within ~35 Ma of Solar System formation leading to
368 degassing into the atmosphere (Marty and Marti, 2002).

369

370 4.3 Comparison to ^{142}Nd - ^{143}Nd systematics of shergottites

371 Previous studies have used the coupled ^{142}Nd - ^{143}Nd chronometry of shergottites to argue for a
372 prolonged interval of martian silicate differentiation and magma ocean crystallisation of up to ~60–
373 100 Ma (Borg et al., 2016; Debaille et al., 2007). Such a late differentiation of Mars contrasts with the
374 evidence for earlier differentiation at ~25–40 Ma inferred in the present study, raising the question as
375 to why these two estimates disagree. Differentiation ages from ^{142}Nd - ^{143}Nd data are typically calculated
376 using two different approaches. First, the ^{142}Nd - ^{143}Nd systematics of *individual* rock samples can be
377 used to calculate three-stage model ages. This approach requires an assumption about the bulk
378 $^{142}\text{Nd}/^{144}\text{Nd}$ of Mars. For instance, assuming that bulk Mars has a ^{142}Nd of -0.06 (*i.e.*, similar to the
379 Earth's mantle) results in model ages of ~60 Ma for the shergottites (Borg et al., 2016). By contrast,
380 assuming an ordinary chondrite-like bulk ^{142}Nd for Mars results in ^{142}Nd model ages of ~30 Ma for
381 the depleted shergottites, and of >100 Ma after Solar System formation for the enriched shergottites
382 (Debaille et al., 2007). Of note, the 30 Ma model age for the depleted shergottites would be consistent
383 with the timescale of Mars' differentiation inferred above using combined ^{142}Nd - ^{182}W systematics
384 (Section 4.2). However, in this case enriched and depleted shergottites would not define a single
385 isochron, that is, their sources would not have formed contemporaneously.

386 In the second approach, *several* rock samples are combined to calculate a single age from a
387 combined ^{142}Nd - ^{143}Nd isochron. Based on this approach, the shergottites define a ^{142}Nd - ^{143}Nd age of
388 63 ± 6 Ma after Solar System formation (Borg et al., 2016). An important underlying assumption of the
389 ^{142}Nd - ^{143}Nd isochron method is that the enriched and depleted shergottites derive from two
390 complementary and co-genetic sources that had formed contemporaneously and subsequently
391 underwent binary mixing. Supporting evidence for this assumption comes from the geochemical
392 characteristics of the shergottite sources, which are consistent with derivation from a common
393 reservoir (Borg et al., 2003; Borg and Draper, 2003; Elkins-Tanton et al., 2003). However, the results
394 of the present study demonstrate that shergottites do not plot on a single mixing array in ^{142}Nd vs.
395 ^{182}W space (Fig. 3), precluding that the shergottites derive from mantle sources that formed
396 concurrently and subsequently mixed. Instead, the ^{182}W - ^{142}Nd systematics of the shergottites require a
397 more protracted interval of source formation between ~ 20 - 25 and ~ 40 Ma after Solar System
398 formation (Fig. 3). A corollary of this is that the ^{142}Nd - ^{143}Nd correlation is not an isochron, but instead
399 a mixing line between sources that likely did not form contemporaneously.

400 Further support for this protracted interval of source formation comes from the ^{182}W - ^{142}Nd
401 systematics of NWA 7034 and ALH 84001. As is evident from their less radiogenic ^{182}W and ^{142}Nd
402 compositions (Fig. 3,4), both ALH 84001 and NWA 7034 derive from sources that were either more
403 strongly enriched or formed earlier than the source of the enriched shergottites. Moreover, the ALH
404 84001 and NWA 7034 sources formed at different times (Fig. 3), demonstrating there is no single
405 enriched component in Mars. As such, the enriched shergottite source may neither be directly related
406 to the residual liquid of a magma ocean, nor to a single enriched component formed at a well-defined
407 point in time during Mars' primordial differentiation. Figure 3 shows that the W and Nd isotopic
408 composition of the enriched shergottites may instead reflect a mixture of depleted and enriched
409 components formed between ~ 25 and ~ 40 Ma after Solar System formation. This implies that the
410 isotopic composition of the enriched shergottites themselves does not provide direct information on
411 the timing of Mars' early differentiation.

412

413 4.4 Nucleosynthetic Nd isotope anomaly in martian meteorites

414 A further complication in the chronological interpretation of ^{142}Nd data is the potential presence
415 of nucleosynthetic Nd isotope variations. Such variations have recently been demonstrated to exist at
416 the bulk planetary scale, leading for instance to different ^{142}Nd compositions of chondrites and the
417 Earth's mantle (Burkhardt et al., 2016). It is currently unknown, however, to what extent Mars
418 exhibits a nucleosynthetic Nd isotope anomaly. Of note, several of the martian samples analysed in
419 this study and in Borg et al. (2016) exhibit small excesses in ^{145}Nd , ^{148}Nd , and ^{150}Nd (Fig. S1; Table
420 S3). However, for individual data points, these apparent excesses are not resolved from the terrestrial
421 standard when taking into account the external reproducibility of the Nd isotope analyses (Section
422 S5). Nevertheless, given that Mars is a differentiated planetary body, any nucleosynthetic isotope
423 signature should be homogeneously distributed within the planet. Thus, in case of Mars, we can pool
424 the non-radiogenic Nd isotope data for individual martian meteorites together to obtain a mean
425 composition for Mars. This approach results in weighted mean values for Mars of $^{148}\text{Nd} = +0.05 \pm 0.02$
426 and $^{150}\text{Nd} = +0.14 \pm 0.10$, $^{145}\text{Nd} = +0.02 \pm 0.03$ (95% conf., N=16). The relative magnitude of these
427 variations is generally consistent with those predicted for nucleosynthetic Nd isotope heterogeneity
428 (Fig. 6; see also Burkhardt et al., 2016). As a result, the Nd isotope composition of Mars may be
429 intermediate between those of enstatite and ordinary chondrites (Fig. 6), consistent with evidence
430 from O and Cr isotopes (Trinquier et al., 2007).

431 The potential presence of nucleosynthetic Nd isotope anomalies in Mars complicates the
432 chronological interpretation of the ^{142}Nd - ^{143}Nd systematics. Although the ^{142}Nd - ^{143}Nd isochron method
433 does not directly depend on an assumed bulk composition of Mars, the assumption of
434 contemporaneous source formation requires that bulk Mars plots on the ^{142}Nd - ^{143}Nd isochron defined
435 by the shergottites (Fig. 7a). By contrast, if Mars had a Nd isotope composition that is intermediate
436 between the compositions of enstatite and ordinary chondrites (as inferred above), then the ^{142}Nd
437 composition of bulk Mars would be between *ca.* -0.10 (enstatite chondrites) and *ca.* -0.18 (ordinary
438 chondrites) (Burkhardt et al., 2016). This inferred bulk composition only marginally overlaps with the
439 bulk Mars ^{142}Nd composition of -0.06 ± 0.07 as inferred from intersection of the ^{142}Nd - ^{143}Nd shergottite
440 array with the chondritic $^{147}\text{Sm}/^{144}\text{Nd}$ ratio (Borg et al. 2016). In this case, the different groups of

441 shergottites would not define a single isochron in ^{142}Nd vs. ^{143}Nd space, but instead be derived from
442 sources that formed at slightly different times (Fig. 7b). Of note, Debaille et al. (2007) assumed an
443 ordinary chondrite-like ^{142}Nd and with this assumption derived an ~ 30 Ma age for the formation of
444 the depleted shergottite source, consistent with the timescale determined in the present study based on
445 combined ^{182}W - ^{142}Nd systematics. Thus, a nucleosynthetic Nd isotope anomaly for Mars provides an
446 alternative way of reconciling the Sm-Nd data of shergottites with the early silicate differentiation of
447 Mars required by the large ^{182}W variations among shergottites. Clearly, fully assessing the extent of
448 nucleosynthetic Nd isotope anomalies in martian meteorites, and their bearing on Sm-Nd chronology,
449 will be an important future task for applying ^{142}Nd - ^{143}Nd systematics to date the early differentiation of
450 Mars.

451

452 **5 Conclusions**

453 Large ^{182}W variations among martian meteorites require silicate differentiation on Mars within
454 20–40 million years after Solar System formation and, hence, earlier than previously inferred based
455 on ^{146}Sm - ^{142}Nd systematics of shergottites alone. The ^{182}W and ^{142}Nd compositions of ALH 84001 and
456 NWA 7034 are the least radiogenic compositions yet reported for martian rocks, indicating that these
457 samples derive from the most strongly enriched sources known from Mars. The combined ^{182}W - ^{142}Nd
458 systematics are inconsistent with a single differentiation event and provide evidence that the initial
459 magma ocean crystallisation was followed by re-melting and crust formation, perhaps triggered by
460 cumulate overturn in the martian mantle. As such the ^{182}W - ^{142}Nd data indicate magma ocean
461 crystallisation on Mars within 20–25 Ma, followed by on-going crust formation until at least ~ 40 Ma
462 after Solar System formation (Fig. 5). These timescales are consistent with Xe isotopic evidence for
463 large-scale degassing at ~ 35 Ma after Solar System formation. Thus, collectively these data
464 demonstrate that Mars underwent a major episode of mantle differentiation, crust formation and
465 atmosphere degassing between ~ 20 and ~ 40 Ma after Solar System formation.

466

467 **Acknowledgements:** NASA and the Meteorite Working Group are gratefully acknowledged for
468 providing several Antarctic meteorite samples for this study, and the UNM Meteorite Museum for
469 providing samples of NWA 7034 and NWA 8159. We thank Richard Walker, Tim Elliott, and Alex
470 Halliday for their constructive and very helpful reviews, and Derek Vance for his editorial efforts.
471 Celeste Brennecka is acknowledged for comments on the manuscript. This study was performed
472 under the auspices of the US DOE by Lawrence Livermore National Laboratory under Contract DE-
473 AC52-07NA27344 with release number LLNL-JRNL-72834. This work was funded by the Deutsche
474 Forschungsgemeinschaft (SFB-TRR 170, subproject C3-1). This is TRR 170 publication no. 24.

475

476 **References:**

- 477 Agee, C.B., Wilson, N. V, McCubbin, F.M., Ziegler, K., Polyak, V.J., Sharp, Z.D., Asmerom, Y.,
478 Nunn, M.H., Shaheen, R., Thiemens, M.H., Steele, A., Fogel, M.L., Bowden, R., Glamoclija,
479 M., Zhang, Z., Elardo, S.M., 2013. Unique meteorite from early Amazonian Mars: water-rich
480 basaltic breccia Northwest Africa 7034. *Science* 339, 780–5. doi:10.1126/science.1228858
- 481 Andreasen, R., Lapen, T.J., Righter, M., Irving, A.J., 2015. Constraints on the Isotopic Composition
482 of the Shergottite Mantle Sources — From Observation Based on the Expanding Rock Record,
483 in: *Lunar and Planetary Science Conference #2976. LPSC 2015.*
- 484 Borg, L.E., Brennecka, G.A., Symes, S.J.K., 2016. Accretion timescale and impact history of Mars
485 deduced from the isotopic systematics of martian meteorites. *Geochim. Cosmochim. Acta* 175,
486 150–167. doi:10.1016/j.gca.2015.12.002
- 487 Borg, L.E., Draper, D.S., 2003. A petrogenetic model for the origin and compositional variation of the
488 martian basaltic meteorites. *Meteorit. Planet. Sci.* 38, 1713–1731. doi:10.1111/j.1945-
489 5100.2003.tb00011.x
- 490 Borg, L.E., Nyquist, L.E., Taylor, L.A., Wiesmann, H., Shih, C.-Y., 1997. Constraints on Martian
491 differentiation processes from Rb-Sr and Sm-Nd isotopic analyses of the basaltic shergottite
492 QUE 94201. *Geochim. Cosmochim. Acta* 61, 4915–4931. doi:10.1016/S0016-7037(97)00276-7
- 493 Borg, L.E., Nyquist, L.E., Wiesmann, H., Shih, C.-Y., Reese, Y., 2003. The age of Dar al Gani 476
494 and the differentiation history of the martian meteorites inferred from their radiogenic isotopic

495 systematics. *Geochim. Cosmochim. Acta* 67, 3519–3536. doi:10.1016/S0016-7037(03)00094-2

496 Boyet, M., Carlson, R.W. (2005) ^{142}Nd Evidence for Early (>4.53 Ga) Global Differentiation of the
497 Silicate Earth. *Science* 309, 576-581.

498 Bouvier A., Boyet, M. (2016) Primitive Solar System materials and Earth share a common initial
499 ^{142}Nd abundance. *Nature* 537, 399-402.

500 Bouvier, A., Vervoort, J.D., Patchett, P.J., 2008. The Lu–Hf and Sm–Nd isotopic composition of
501 CHUR: Constraints from unequilibrated chondrites and implications for the bulk composition of
502 terrestrial planets, *Earth and Planetary Science Letters*. doi:10.1016/j.epsl.2008.06.010

503 Brennecka, G.A., Borg, L.E., Wadhwa, M., 2014. Insights into the Martian mantle: The age and
504 isotopics of the meteorite fall Tissint. *Meteorit. Planet. Sci.* 49, 412–418.
505 doi:10.1111/maps.12258

506 Budde, G., Kruijer, T.S., Fischer-Gödde, M., Kleine, T., 2015. Planetsimal differentiation revealed
507 by the Hf-W systematics of ureilites. *Earth Planet. Sci. Lett.* 430, 316–325.

508 Burkhardt, C., Borg, L.E., Brennecka, G.A., Shollenberger, Q.R., Dauphas, N., Kleine, T., 2016. A
509 nucleosynthetic origin of the Earth’s anomalous ^{142}Nd composition. *Nature* 537, 394–398.

510 Caro, G., Bourdon, B., Halliday, A.N., Quitté, G., 2008. Super-chondritic Sm/Nd ratios in Mars, the
511 Earth and the Moon. *Nature* 452, 336–9. doi:10.1038/nature06760

512 Campbell, I. H., O’Neill, H. S. C. (2012) Evidence against a chondritic Earth. *Nature* 483, 553–558.

513 Cook, D.L., Schönbachler, M., 2016. High-precision measurement of W isotopes in Fe–Ni alloy and
514 the effects from the nuclear field shift. *J. Anal. At. Spectrom.* 31, 1400–1405.
515 doi:10.1039/C6JA00015K

516 Dauphas, N., Pourmand, A., 2011. Hf-W-Th evidence for rapid growth of Mars and its status as a
517 planetary embryo. *Nature* 473, 489–92. doi:10.1038/nature10077

518 Debaille, V., Brandon, A.D., O’Neill, C., Yin, Q.-Z., Jacobsen, B., 2009. Early martian mantle
519 overturn inferred from isotopic composition of nakhlite meteorites. *Nat. Geosci.* 2, 548–552.
520 doi:10.1038/ngeo579

521 Debaille, V., Brandon, A.D., Yin, Q.Z., Jacobsen, B., 2007. Coupled ^{142}Nd - ^{143}Nd evidence for a
522 protracted magma ocean in Mars. *Nature* 450, 525–8. doi:10.1038/nature06317

523 Debaille, V., Yin, Q.-Z., Brandon, A.D., Jacobsen, B., 2008. Martian mantle mineralogy investigated
524 by the ^{176}Lu – ^{176}Hf and ^{147}Sm – ^{143}Nd systematics of shergottites. *Earth Planet. Sci. Lett.* 269,
525 186–199. doi:10.1016/j.epsl.2008.02.008

526 Elkins-Tanton, L.T., 2008. Linked magma ocean solidification and atmospheric growth for Earth and
527 Mars. *Earth Planet. Sci. Lett.* 271, 181–191. doi:10.1016/j.epsl.2008.03.062

528 Elkins-Tanton, L.T., 2005. Possible formation of ancient crust on Mars through magma ocean
529 processes. *J. Geophys. Res.* 110, E12S01. doi:10.1029/2005JE002480

530 Elkins-Tanton, L.T., Parmentier, E.M., Hess, P.C., 2003. Magma ocean fractional crystallisation and
531 cumulate overturn in terrestrial planets: Implications for Mars. *Meteorit. Planet. Sci.* 38, 1753–
532 1771.

533 Foley, C.N., Wadhwa, M., Borg, L.E., Janney, P.E., Hines, R., Grove, T.L., 2005. The early
534 differentiation history of Mars from ^{182}W – ^{142}Nd isotope systematics in the SNC meteorites.
535 *Geochim. Cosmochim. Acta* 69, 4557–4571. doi:10.1016/j.gca.2005.05.009

536 Humayun, M., Nemchin, A., Zanda, B., Hewins, R.H., Grange, M., Kennedy, A., Lorand, J.-P.,
537 Göpel, C., Fieni, C., Pont, S., Deldicque, D., 2013. Origin and age of the earliest Martian crust
538 from meteorite NWA 7533. *Nature* 503, 513–6. doi:10.1038/nature12764

539 Jacobsen, S.B., Wasserburg, G.J., 1980. Sm–Nd isotopic composition of chondrites. *Earth Planet. Sci.*
540 *Lett.* 50, 139–156.

541 Kleine, T., Hans, U., Irving, A.J., Bourdon, B., 2012. Chronology of the angrite parent body and
542 implications for core formation in protoplanets. *Geochim. Cosmochim. Acta* 84, 186–203.
543 doi:10.1016/j.gca.2012.01.032

544 Kleine, T., Mezger, K., Münker, C., Palme, H., Bischoff, A., 2004. ^{182}Hf – ^{182}W isotope systematics
545 of chondrites, eucrites, and martian meteorites: Chronology of core formation and early mantle
546 differentiation in Vesta and Mars. *Geochim. Cosmochim. Acta* 68, 2935–2946.
547 doi:10.1016/j.gca.2004.01.009

548 Kleine, T., Touboul, M., Bourdon, B., Nimmo, F., Mezger, K., Palme, H., Jacobsen, S.B., Yin, Q.-Z.,
549 Halliday, A.N., 2009. Hf–W chronology of the accretion and early evolution of asteroids and
550 terrestrial planets. *Geochim. Cosmochim. Acta* 73, 5150–5188. doi:10.1016/j.gca.2008.11.047

551 Kruijer, T.S., Kleine, T., Fischer-Gödde, M., Burkhardt, C., Wieler, R., 2014. Nucleosynthetic W
552 isotope anomalies and the Hf-W chronometry of Ca-Al-rich inclusions. *Earth Planet. Sci. Lett.*
553 403, 317–327. doi:10.1016/j.epsl.2014.07.003

554 Kruijer, T.S., Kleine, T., Fischer-Gödde, M., Sprung, P., 2015. Lunar tungsten isotopic evidence for
555 the late veneer. *Nature* 520, 534–537. doi:10.1038/nature14360

556 Kruijer, T.S., Sprung, P., Kleine, T., Leya, I., Burkhardt, C., Wieler, R., 2012. Hf-W chronometry of
557 core formation in planetesimals inferred from weakly irradiated iron meteorites. *Geochim.*
558 *Cosmochim. Acta* 99, 287–304. doi:10.1016/j.gca.2012.09.015

559 Lapen, T.J., Righter, M., Andreasen, R., Irving, A.J., Satkoski, A.M., Beard, B.L., Nishiizumi, K.,
560 Jull, A.J.T., Caffee, M.W., 2017. Two billion years of magmatism recorded from a single Mars
561 meteorite ejection site. *Sci. Adv.* 3.

562 Lapen, T.J., Righter, M., Brandon, A.D., Debaille, V., Beard, B.L., Shafer, J.T., Peslier, A.H., 2010.
563 A younger age for ALH84001 and its geochemical link to shergottite sources in Mars. *Science*
564 328, 347–51. doi:10.1126/science.1185395

565 Lee, D.-C., Halliday, A.N., 1997. Core formation on Mars and differentiated asteroids. *Nature* 388,
566 854–857.

567 Meyer C. The Martian meteorite compendium. Available at <https://curator.jsc.nasa.gov/antmet/mmc/>.

568 Marty, B., Marti, K., 2002. Signatures of early differentiation of Mars. *Earth Planet. Sci. Lett.* 196,
569 251–263. doi:10.1016/S0012-821X(01)00612-4

570 Mezger, K., Debaille, V., Kleine, T., 2013. Core Formation and Mantle Differentiation on Mars.
571 *Space Sci. Rev.* 174, 27–48. doi:10.1007/s11214-012-9935-8

572 Morishima, R., Golabek, G.J., Samuel, H., 2013. N-body simulations of oligarchic growth of Mars:
573 Implications for Hf-W chronology. *Earth Planet. Sci. Lett.* 366, 6–16.
574 doi:10.1016/j.epsl.2013.01.036

575 Nimmo, F., Kleine, T., 2007. How rapidly did Mars accrete? Uncertainties in the Hf-W timing of
576 core formation. *Icarus* 191, 497–504. doi:10.1016/j.icarus.2007.05.002

577 Nyquist, L.E., Shih, C.-Y., McCubbin, F.M., Santos, A.R., Shearer, C.K., Peng, Z.X., Burger, P. V.,
578 Agee, C.B., 2016. Rb-Sr and Sm-Nd isotopic and REE studies of igneous components in the

579 bulk matrix domain of Martian breccia Northwest Africa 7034. *Meteorit. Planet. Sci.* 51, 483–
580 498. doi:10.1111/maps.12606

581 Righter, K., Chabot, N.L., 2011. Moderately and slightly siderophile element constraints on the depth
582 and extent of melting in early Mars. *Meteorit. Planet. Sci.* 46, 157–176. doi:10.1111/j.1945-
583 5100.2010.01140.x

584 Righter, K., Shearer, C.K., 2003. Magmatic fractionation of Hf and W: constraints on the timing of
585 core formation and differentiation in the Moon and Mars. *Geochim. Cosmochim. Acta* 67,
586 2497–2507. doi:10.1016/S0016-7037(02)01349-2

587 Snyder, G.A., Taylor, L.A., Neal, C.R., 1992. A chemical model for generating the sources of mare
588 basalts: Combined equilibrium and fractional crystallisation of the lunar magmasphere.
589 *Geochim. Cosmochim. Acta* 56, 3809–3823. doi:10.1016/0016-7037(92)90172-F

590 Trinquier, A., Birck, J-L, Allègre, C.J., 2007. Widespread ^{54}Cr heterogeneity in the inner Solar
591 System. *Astrophys. J.* 655:1179-1185.

592 Willbold, M., Elliott, T., Moorbath, S., 2011. The tungsten isotopic composition of the Earth's mantle
593 before the terminal bombardment. *Nature* 477, 195–8. doi:10.1038/nature10399

594

595

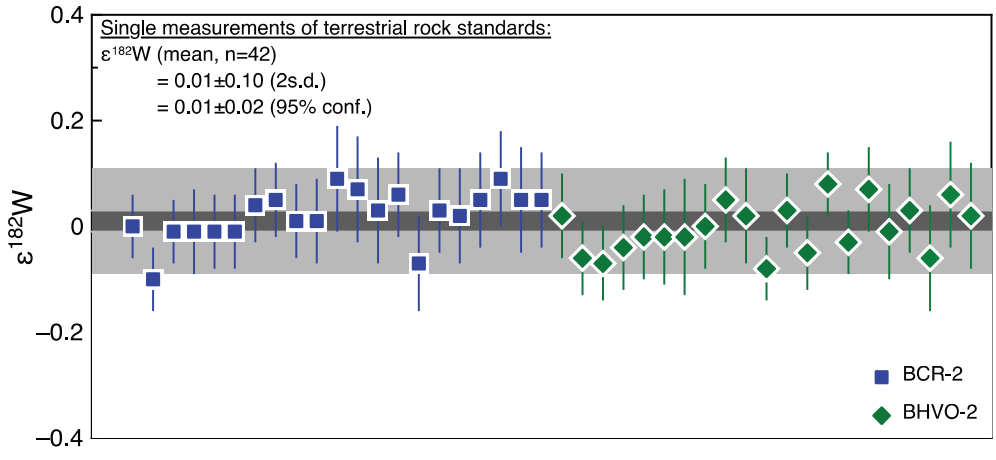
Table 1**Tungsten and Nd isotope data for martian meteorites.**

Sample	<i>N</i>	$\epsilon^{182}\text{W}$ ($\pm 2\sigma$)	$\epsilon^{142}\text{Nd}$ ($\pm 2\sigma$)
Enriched shergottites			
Zagami	3	0.35 \pm 0.10	ND
RBT 04262	2	0.42 \pm 0.10	ND
NWA 4864	1	0.35 \pm 0.10	-0.19 \pm 0.06
LAR 12011	2	0.33 \pm 0.10	-0.13 \pm 0.06
NWA 4468 *	3	0.40 \pm 0.10	-0.17 \pm 0.06
Mean (\pm 95% conf., n=5)		0.37 \pm 0.05	-0.16 \pm 0.08
Intermediate shergottites			
EETA 79001B *	2	0.29 \pm 0.10	0.23 \pm 0.06
ALH 77005 *	1	0.51 \pm 0.12	0.16 \pm 0.07
NWA 7042	2	0.37 \pm 0.10	0.03 \pm 0.06
Depleted shergottites			
SaU 005 *	1	0.83 \pm 0.10	0.57 \pm 0.06
LAR 12095	1	0.90 \pm 0.16	ND
DaG 476 *	1	0.91 \pm 0.10	0.65 \pm 0.06
Tissint	1	1.48 \pm 0.10	0.72 \pm 0.06
NWA 7635 §	1	1.80 \pm 0.13	0.92 \pm 0.08
Orthopyroxenite			
ALH 84001	1	0.09 \pm 0.10	
ALH 84001 (<i>replicate</i>)	1	0.08 \pm 0.10	
ALH 84001 (Mean)		0.09 \pm 0.10	-0.29 \pm 0.06
Polymict breccia			
NWA 7034 (\pm 95% conf.)	5	0.20 \pm 0.05	-0.45 \pm 0.06
Augite basalt			
NWA 8159	1	1.13 \pm 0.10	0.77 \pm 0.06

597 ^{182}W data analysed by MC-ICPMS and ^{142}Nd data by TIMS (See Supplementary Material). *N*,
598 number of W isotope measurements of each sample; ND, not determined. ^{182}W internally normalised
599 to $^{186}\text{W}/^{184}\text{W} = 0.92767$, and ^{142}Nd to $^{146}\text{Nd}/^{144}\text{Nd} = 0.7219$. Uncertainties on ^{182}W and ^{142}Nd represent
600 the external reproducibility (2s.d.) estimated from rock standard analyses from this study (Table S1),
601 or the two-standard error (2s.e.) obtained from internal run statistics, whichever is larger. * ^{142}Nd data
602 from Borg et al. (2016), in case of EETA 79001, determined on lithology A. § ^{142}Nd data from Lapen
603 et al. (2017).

604

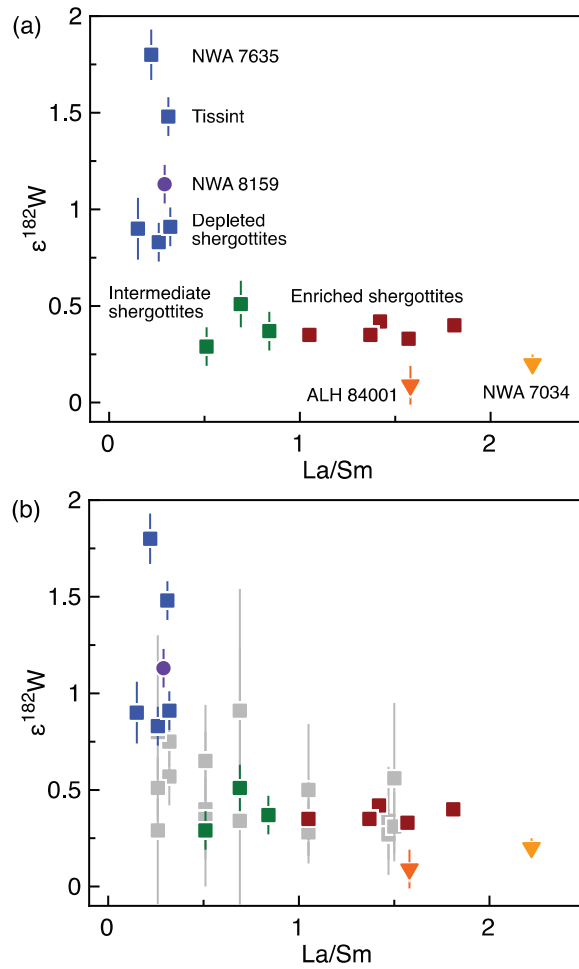
605



607

608 **Fig. 1:** ^{182}W data for the silicate rock standards analyzed in this study. Each data point represents
 609 a single W isotope measurement of a standard that was processed through the full chemical separation
 610 and error bars denote internal errors (2s.e.). The external uncertainty (2 s.d.), as inferred from
 611 replicate standard analyses, is shown as a light grey filled bar, and the corresponding 95% confidence
 612 interval as a dark grey bar.

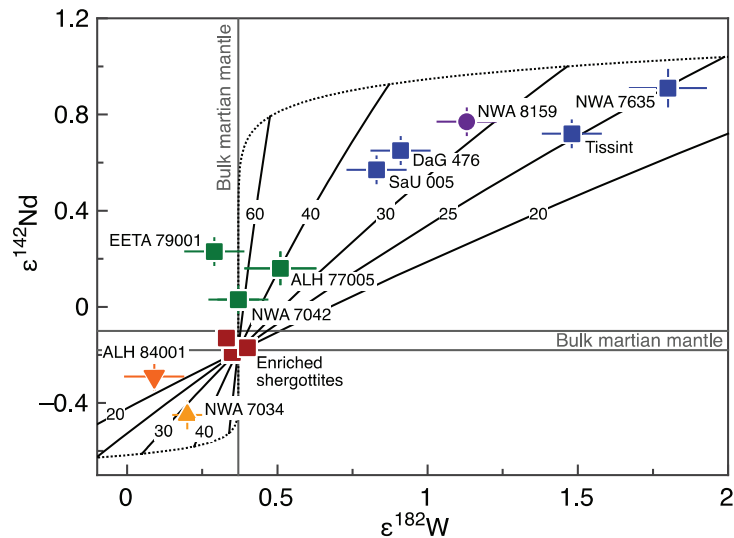
613



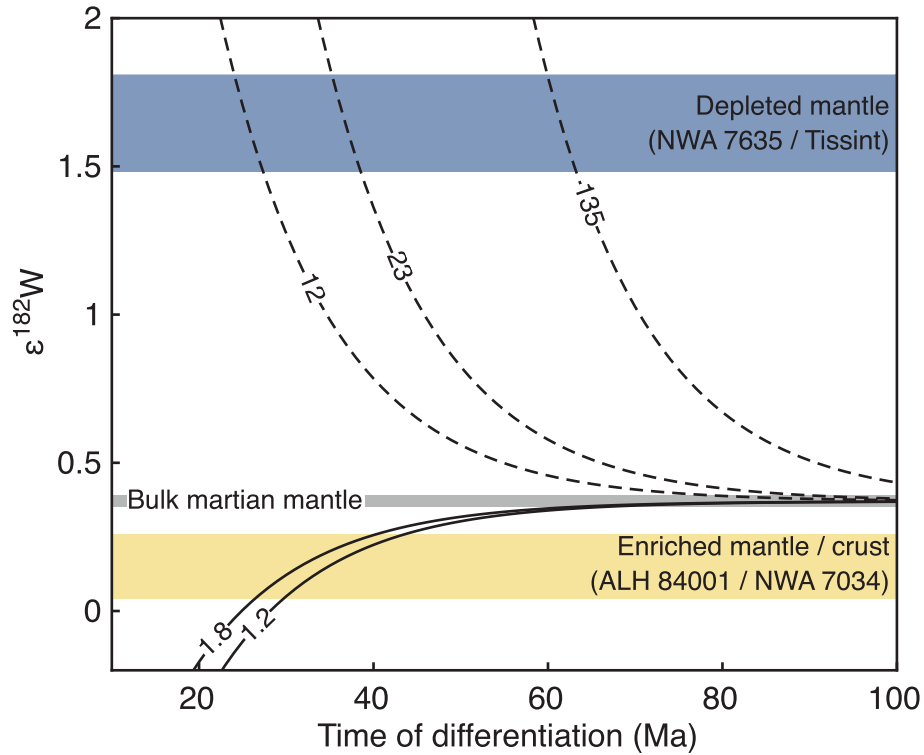
614

615 **Fig. 2:** ^{182}W data of martian meteorites plotted vs. La/Sm as an index for enrichment. (a) samples
 616 analysed in this study, and (b) data shown in comparison to literature ^{182}W data (light grey squares;
 617 Lee and Halliday, 1997; Kleine et al., 2004; Foley et al., 2005). Error bars indicate external
 618 uncertainties (2 σ , see Table S2 and Supplementary Material). Data sources for La/Sm ratios: The
 619 martian meteorite compendium (and references therein), Humayun et al. (2013), and Lapen et al.
 620 (2017).

621



623 **Fig. 3:** Coupled ^{182}W vs. ^{142}Nd systematics of martian meteorites. The coupled ^{182}W – ^{142}Nd data
 624 are shown together with model results for magma ocean crystallisation (see Supplementary material).
 625 Dotted line shows ^{182}W – ^{142}Nd composition of the enriched (*lower left quadrant*) and the depleted
 626 mantle end member (*upper right quadrant*) after magma ocean crystallisation of a primordial mantle.
 627 Solid curved lines represent mixing lines between end member sources formed at different times after
 628 Solar System formation (*i.e.*, at 20, 25, 30, 40 and 60 Ma). Grey horizontal and vertical lines show the
 629 ^{182}W and ^{142}Nd compositions of the bulk martian mantle as inferred in this study. Existing data for
 630 nakhlites are not plotted because their source(s) had a more complex history, involving more than two
 631 stages of evolution (Righter and Shearer, 2003; Kleine et al., 2004; Foley et al., 2005; Debaille et al.,
 632 2009). As a consequence, no meaningful age information can be deduced for the nakhlites using the
 633 two-stage model illustrated here. Note that one sample (EETA 79001) plots outside the field of
 634 possible differentiation ages, either reflecting that ^{182}W and ^{142}Nd were not determined on the same
 635 lithologies, or that crustal contamination modified ^{182}W and ^{142}Nd to different degrees (Andreasen et
 636 al., 2015).



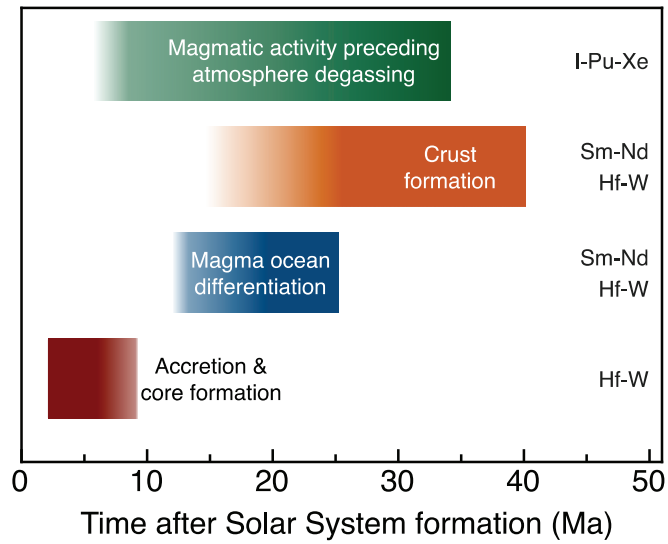
637

638 **Fig. 4:** Timescales of martian mantle differentiation inferred from Hf-W systematics. Shaded areas
 639 denote the range in ^{182}W measured for martian meteorites from enriched (ALH 84001, NWA 7034)
 640 and the most depleted mantle sources (NWA 7635, Tissint). Model curves show the possible range in
 641 ^{182}W of enriched (*solid lines*) and depleted (*dashed lines*) mantle sources produced by magma ocean
 642 crystallisation as a function of differentiation time. These model ^{182}W compositions were calculated
 643 using the range in Hf/W obtained for enriched ($^{180}\text{Hf}/^{184}\text{W} = 1.2\text{-}1.8$) and depleted ($^{180}\text{Hf}/^{184}\text{W} = 12\text{-}23$)
 644 end member sources from the magma ocean model (see Supplementary Material). The ^{182}W
 645 composition of the bulk martian mantle (*grey shaded bar*) is shown for reference.

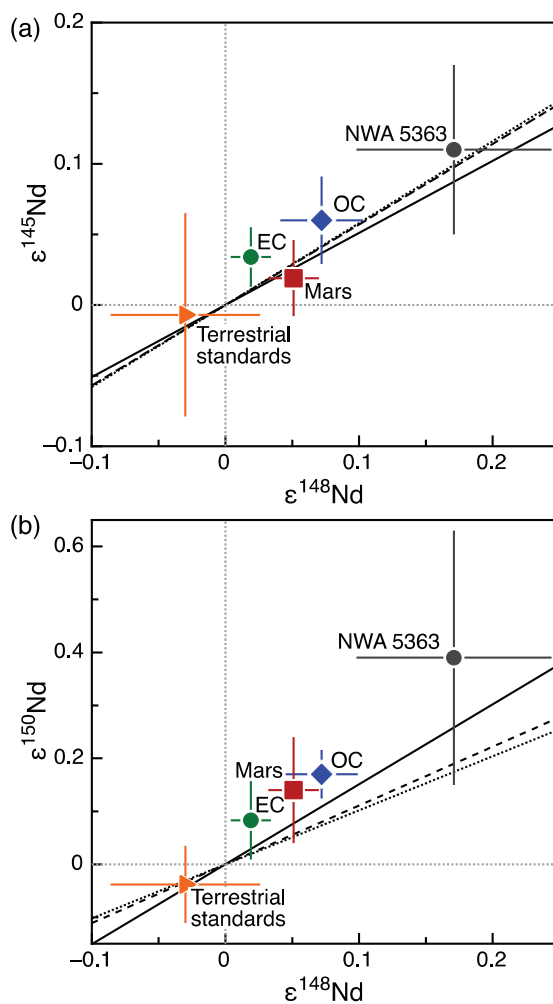
646

647

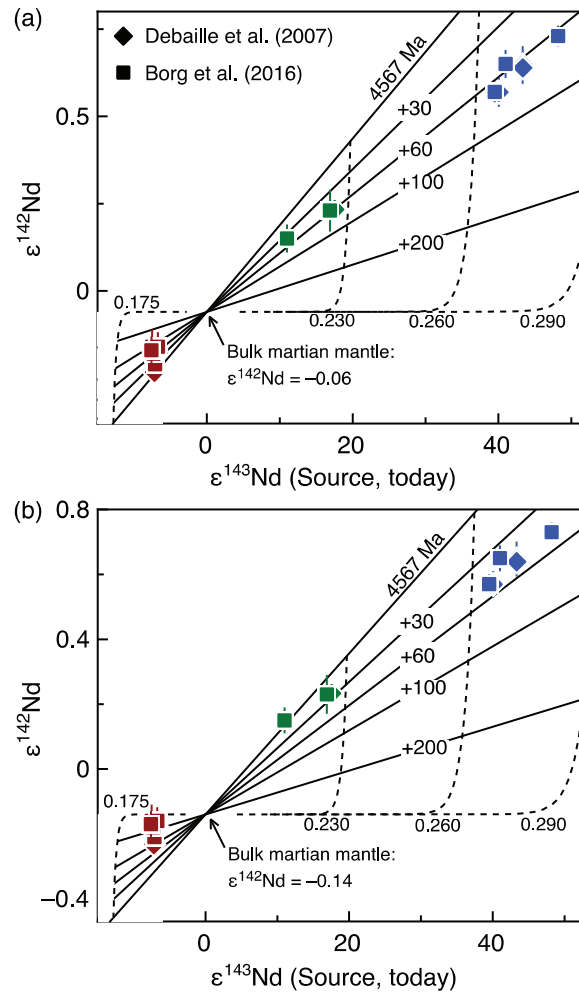
648



649 **Fig. 5:** Chronology for the early differentiation of Mars. Shown are the timing of accretion and
650 core formation as inferred using Hf-W chronometry (Dauphas and Pourmand, 2011; Kleine et al.,
651 2004; Nimmo and Kleine, 2007), the new estimates for the timescales of magma ocean differentiation
652 and crust formation from this study, and the timing of magmatic activity as required to explain the I-
653 Pu-Xe systematics of martian meteorites (Marty and Marti, 2002).
654



656 **Fig. 6:** Non-radiogenic Nd isotope compositions of meteorites. (a) ^{145}Nd vs. ^{148}Nd and (b) ^{150}Nd
 657 vs. ^{148}Nd . The data point for Mars represents the mean value obtained for martian meteorites from this
 658 study and from (Borg et al., 2016), while data for ordinary chondrites, enstatite chondrites and NWA
 659 5363 are from Burkhardt et al. (2016). Also shown are mixing lines between *s*-process Nd and
 660 terrestrial Nd, as described in Burkhardt et al. (2016).
 661



663

664 **Fig. 7:** ^{142}Nd - ^{143}Nd isochron diagram used to determine the age of shergottite source regions.
 665 Measured ^{142}Nd of shergottites (*solid symbols*) are plotted vs. the ^{143}Nd of the present-day sources,
 666 calculated using the initial $^{143}\text{Nd}/^{144}\text{Nd}$ of each meteorite, and the approach described in Borg et al.
 667 (2016). Solid lines show model isochrons for source formation at 30, 60, 100, and 200 Ma after CAI
 668 formation. The model isochrons were calculated using two different ^{142}Nd values for the bulk martian
 669 mantle: (a) using ^{142}Nd of -0.06 ± 0.07 (Borg et al. (2016), in the case that Mars has no
 670 nucleosynthetic Nd isotope anomaly relative to the Earth, and in (b) using ^{142}Nd of ~ -0.14 , in the case
 671 that Mars has a nucleosynthetic Nd isotope anomaly between that of enstatite and ordinary chondrites
 672 (see main text). Vertical dotted lines show the Nd isotope evolution for different source $^{147}\text{Sm}/^{144}\text{Nd}$
 673 (0.175, 0.23, 0.26, and 0.29). Neodymium isotope data of shergottites are from Debaïlle et al. (2007)
 674 and Borg et al. (2016).